

## Tight-binding Electronic Structure Study of the $\beta'$ - and $\beta''$ -Phases of the Organic Conducting Salts $(\text{BEDT-TTF})_2[(\text{IBr}_2)_{0.2}(\text{BrICl})_{0.1}(\text{ICl}_2)_{0.7}]$

Hyun-Joo Koo\* and Myung-Hwan Whangbo<sup>†,\*</sup>

Department of Chemistry and Research Institute of Basic Science, Kyung Hee University, Seoul 130-701, Korea

\*E-mail: hjkoo@khu.ac.kr

<sup>†</sup>Department of Chemistry, North Carolina State University, Raleigh, North Carolina 27695-8204, USA

\*E-mail: mike\_whangbo@ncsu.edu

Received October 31, 2006

The electronic structures of the new organic conducting salts, the  $\beta'$ - and  $\beta''$ -phases of  $(\text{BEDT-TTF})_2[(\text{IBr}_2)_{0.2}(\text{BrICl})_{0.1}(\text{ICl}_2)_{0.7}]$ , were examined by calculating their electronic band structures, Fermi surfaces and HOMO-HOMO interaction energies using the extended Hückel tight binding method. On the basis of these calculations, we probed why the  $\beta'$ -phase is semiconducting while the  $\beta''$ -phase is metallic.

**Key Words** : Organic conducting salt, BEDT-TTF, Electronic structure calculations, HOMO-HOMO interaction energy

### Introduction

A large number of organic metals and superconductors have been found from the 2 : 1 salts,  $(\text{BEDT-TTF})_2\text{X}$ , of the donor molecule BEDT-TTF with monovalent anions  $\text{X}^-$ , where BEDT-TTF (or simply ET) refers to bis(ethylenedithio)tetrathiafulvalence.<sup>1</sup> These salts have a crystal structure in which layers of ET molecules are separated by layers of monovalent anions  $\text{X}^-$ . A small modification in the anion structure induces a change in the packing motif of the donor molecule layer, the interactions between nearest-neighbor ET molecules, and hence a profound change in the physical properties of the 2 : 1 salts. For example, the  $\beta$ - $(\text{ET})_2\text{X}$  salts with linear triatomic anions  $\text{X}^- = \text{I}_3^-$ ,  $\text{IBr}_2^-$  and  $\text{AuI}_2^-$  are superconductors, with the highest  $T_c$  obtained for the longest anion  $\text{I}_3^-$ .<sup>2,3</sup> With shorter linear anions  $\text{X}^- = \text{ICl}_2^-$  and  $\text{AuCl}_2^-$ , the  $\beta$ - $(\text{ET})_2\text{X}$  salts are magnetic semiconductors and undergo a three-dimensional antiferromagnetic phase transition at low temperatures.<sup>4,6</sup> Many of ET salts prepared with linear triatomic anions exhibit a number of different crystal packing patterns ( $\alpha$ ,  $\beta$ ,  $\kappa$ ,  $\delta$ , etc.) and the  $\beta$ -type salts are further classified into three subgroups, *i.e.*,  $\beta$ ,  $\beta'$  and  $\beta''$ .<sup>1,7</sup>

Recently, the 2 : 1 organic conducting salt  $(\text{ET})_2[(\text{IBr}_2)_{0.2}(\text{BrICl})_{0.1}(\text{ICl}_2)_{0.7}]$  has been reported to have two polymorphs,  $\beta'$ - and  $\beta''$ -phases, which have two crystallographically equivalent ET molecules per unit cell.<sup>8</sup> The ET molecules are stacked face-to-face along the  $(-\mathbf{a}+\mathbf{b})$  direction in the  $\beta'$ -phase, and along the  $\mathbf{b}$ -axis direction in the  $\beta''$ -phase (Figure 1). These stacks form layers of ET molecules parallel to the  $\mathbf{ab}$ -plane, as shown in Figure 1a and 1b for the  $\beta'$ - and  $\beta''$ -phase, respectively. The layers of the ET molecules alternate with the layers of the anions along the  $\mathbf{c}$ -direction.

The electrical resistivity measurements<sup>8</sup> show that the  $\beta'$ -phase of  $(\text{ET})_2[(\text{IBr}_2)_{0.2}(\text{BrICl})_{0.1}(\text{ICl}_2)_{0.7}]$  is a semiconductor with activation energy of 0.076 eV. In contrast, the  $\beta''$ -phase is metallic down to 10 K, but its resistivity increases sharply

below 10 K. The angle dependence of the ESR signal of the  $\beta''$ -phase suggests a nearly isotropic electronic structure in the donor-molecule layer (parallel to the  $\mathbf{ab}$ -plane),<sup>8</sup> which is characteristic of a quasi two-dimensional (2D) organic metal. This 2D character of the electronic structure has been explained by considering the structure of the donor molecule layer of the  $\beta''$ -phase, in which both the intra- and the inter-stack ET  $\cdots$ ET arrangements have S  $\cdots$  S distances shorter than the van der Waals distance.<sup>8</sup> As in the case of  $(\text{ET})_2[(\text{IBr}_2)_{0.2}(\text{BrICl})_{0.1}(\text{ICl}_2)_{0.7}]$ , the  $\beta'$ - and  $\beta''$ -phases of  $(\text{ET})_2(\text{ICl}_2)$  also exhibit contrasting electrical resistivity behaviors: the  $\beta''$ -phase is metallic down to 1.5 K, but the  $\beta'$ -phase is a semiconductor with activation energy greater than 0.076 eV.<sup>8,9</sup>

In understanding the electrical transport properties of organic conducting salts, their band dispersion relations and Fermi surfaces determined by extended Hückel tight binding (EHTB) calculations<sup>10</sup> have been indispensable.<sup>11-15</sup> In the present work, we carry out EHTB electronic structure calculations for the  $\beta'$ - and  $\beta''$ -phases of  $(\text{ET})_2[(\text{IBr}_2)_{0.2}(\text{BrICl})_{0.1}(\text{ICl}_2)_{0.7}]$  to gain insight into why the two polymorphs differ in their electrical transport properties. In the present EHTB calculations, the valence atomic orbitals of C and S atoms in the donor molecules were represented by double-zeta Slater-type orbitals, because the tail part of an atomic orbital is essential in the overlap between adjacent donor molecules.<sup>12,16-18</sup> The atomic orbital parameters employed in the present study are listed in Table 1.

### Electronic Band Structures

Figure 2 shows the band dispersion relations for the two HOMO bands (*i.e.*, the highest two occupied bands derived largely from the HOMO's of the donor molecules) calculated for the  $\beta'$ -phase of  $(\text{ET})_2[(\text{IBr}_2)_{0.2}(\text{BrICl})_{0.1}(\text{ICl}_2)_{0.7}]$ . With the oxidation assignment  $(\text{ET})_2^+\text{X}^-$ , there are three electrons to fill these two bands so that the lower-lying

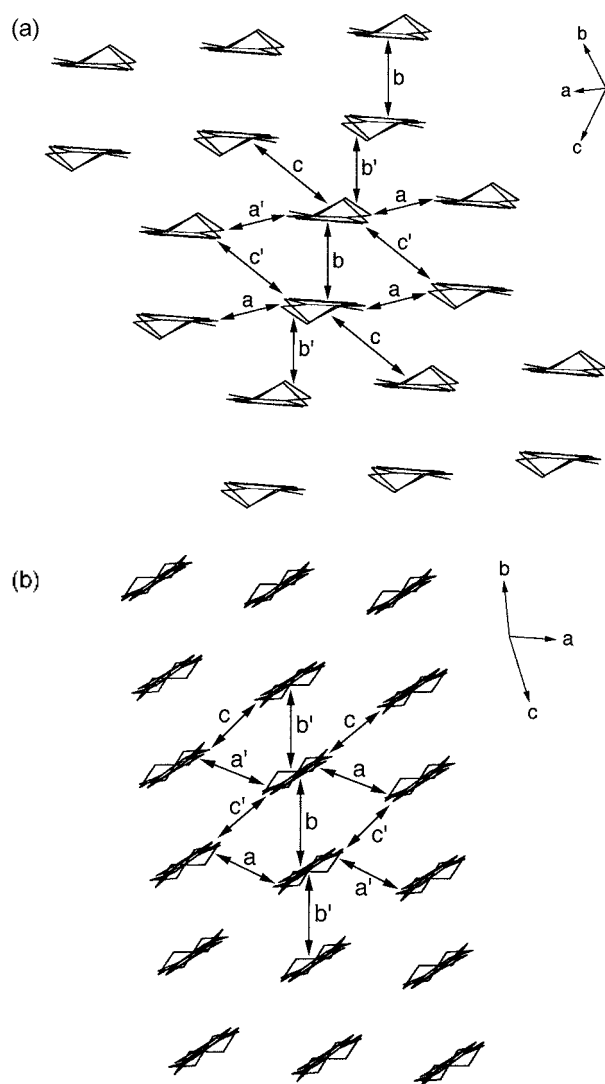


**Figure 1.** Packing patterns of the ET molecules in the donor layer of (a) the  $\beta$ -phase and (b) the  $\beta'$ -phase, where each label between adjacent ET molecules defines the pair of nearest-neighbors ET molecules  $i$  and  $j$ , for which the HOMO-HOMO interaction energy  $\beta_{ij}$  is listed in Table 2.

**Table 1.** Exponents  $\zeta_i$  and valence shell ionization potentials  $H_{ii}$  of Slater-type orbitals  $\chi_i$  used for extended Hückel tight-binding calculation<sup>a</sup>

Atom	$\chi_i$	$H_{ii}$ (eV)	$\zeta_i$	C	$\zeta'_i$	C'
S	2s	-20.0	2.662	0.5990	1.688	0.5246
S	2p	-13.3	2.338	0.5377	1.333	0.5615
C	2s	-21.4	1.831	0.7931	1.153	0.2739
C	2p	-11.4	2.730	0.2595	1.257	0.8026
H	1s	-13.6	1.300	1.0000		

<sup>a</sup> $H_{ii}$ 's are the diagonal matrix elements  $\langle \chi_i | H^{\text{eff}} | \chi_i \rangle$ , where  $H^{\text{eff}}$  is the effective Hamiltonian. In our calculations of the off-diagonal matrix elements  $H_{ij} = \langle \chi_i | H^{\text{eff}} | \chi_j \rangle$ , the weighted formula was used. See: Ammeter, J.; Bürgi, H.-B.; Thibeault, J.; Hoffmann, R. *J. Am. Chem. Soc.* 1978, 100, 3686.

HOMO band is fully occupied while the highest-lying band is half-filled. In Figure 2 the Fermi level is given by assuming the metallic state for the  $\beta'$ -phase, namely, each of the

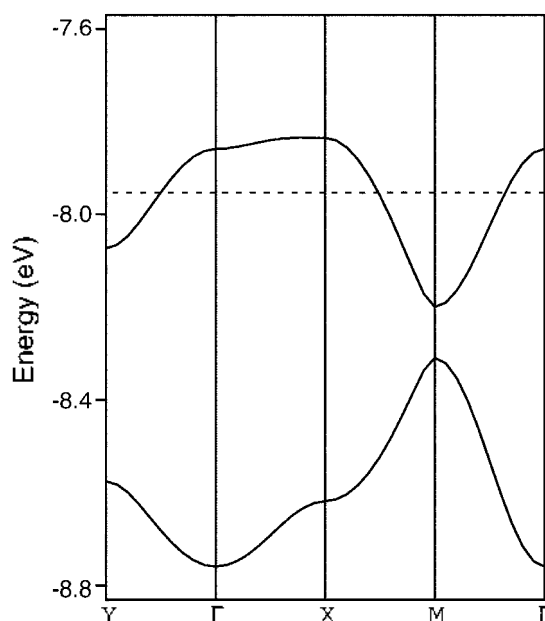


**Figure 2.** Dispersion relations of the two HOMO bands calculated for the  $\beta'$ -phase, where the dashed line refers to the Fermi level,  $\Gamma = (0, 0)$ ,  $X = (a^*/2, 0)$ ,  $Y = (0, b^*/2)$  and  $M = (a^*/2, b^*/2)$ .

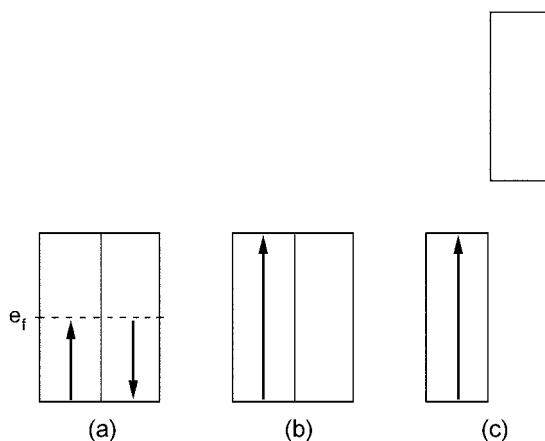


**Figure 3.** Metallic and magnetic insulating states of a half-filled band: (a) Metallic state. (b) Magnetic insulating state in non-spin-polarized representation. (c) Magnetic insulating state in spin-polarized representation.

upper HOMO band levels is doubly filled up to the Fermi level as depicted in Figure 3a. The width of this half filled band is narrow, and the  $\beta$ -phase is not metallic. Therefore, the insulating behavior must arise from electron-electron repulsion, which leads to a magnetic insulating state.<sup>19,20</sup> In the non-spin-polarized band picture, the ferromagnetic insulating state of a half-filled band has each band level singly occupied by an up-spin electron (Figure 3b). In spin-polarized electronic band picture, the completely filled up-spin band is separated from the empty down-spin band by an energy gap (Figure 3c) thereby explaining a non-metallic property.

Figure 4a shows the dispersion relations of the highest two occupied bands calculated for the donor layers of the  $\beta'$ -

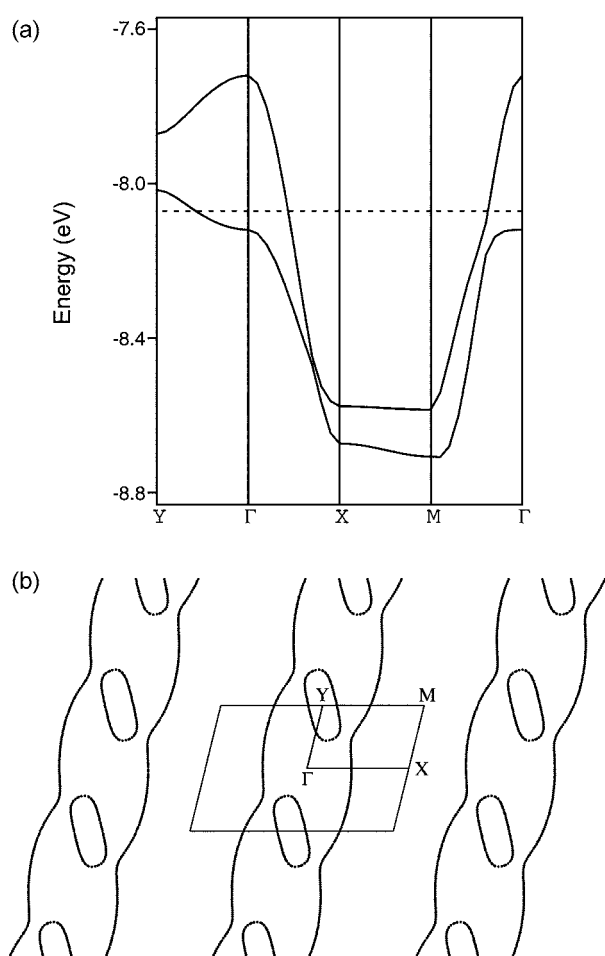


**Figure 4.** (a) Dispersion relations of the two HOMO bands calculated for the  $\beta'$ -phase, where the dashed line refers to the Fermi level,  $\Gamma = (0, 0)$ ,  $X = (a^*/2, 0)$ ,  $Y = (0, b^*/2)$  and  $M = (a^*/2, b^*/2)$ . (b) Fermi surfaces associated with the partially filled bands of Fig. 4a in an extended zone.

phase. The two HOMO bands are partially filled and more dispersive than those of the  $\beta$ -phase. Since the  $\beta'$ -phase is metallic, it is appropriate to consider its metallic state. The lower-lying band is fully occupied along the  $\Gamma \rightarrow X \rightarrow M \rightarrow \Gamma$  but is partially empty around Y, while the highest-lying band is nearly half-filled along the  $\Gamma \rightarrow X$  and  $M \rightarrow \Gamma$  direction. The Fermi surfaces associated with these two HOMO bands are shown in Figure 4b in an extended zone scheme. The Fermi surfaces consist of a closed hole pocket centered at Y and a pair of wavy lines straddling the  $\Gamma \rightarrow Y$  line. Thus, the  $\beta'$ -phase has both one-dimensional (1D) and 2D Fermi surfaces. Topologically, these two kinds of Fermi surfaces originate from overlapping ellipses that inscribe the wavy 1D Fermi surfaces. If one takes into consideration a non-crossing of the curves at each crossing point of the overlapping ellipses, then the 1D and 2D Fermi surfaces are obtained. In other words, the 1D and 2D Fermi surfaces taken together suggest that the electrical conductivity of the  $\beta'$ -phase should be almost isotropic within the plane of the donor molecule layer. This is consistent with conclusion derived from the ESR study of the  $\beta'$ -phase.<sup>8</sup>

### Analysis of HOMO-HOMO Interaction Energies

The relative strengths of the interactions between nearest-neighbor ET molecules in the donor layers of the  $\beta$ - and  $\beta'$ -phases can be estimated by calculating the HOMO-HOMO interaction energies  $\beta_{ij} = \langle \psi_i | H^{eff} | \psi_j \rangle$ ,<sup>22</sup> where  $H^{eff}$  is an effective Hamiltonian, and  $\psi_i$  and  $\psi_j$  are the HOMO's of nearest-neighbor ET molecules *i* and *j*, respectively. Table 2 summarizes the values calculated for the various pairs of ET molecules in the  $\beta$ - and  $\beta'$ -phases shown in Figure 1a and 1b.

The  $\beta_y$  values for the  $\beta$ -phase, listed in Table 2a, show a strong dimerization in the donor-molecule stack. The strongest HOMO-HOMO interaction occurs in the pairs of ET molecules labeled as *b* in Figure 1a. These  $(ET)_2^-$  units contain one unpaired spin and hence should be regarded as spin monomers. To find the spin lattice appropriate for the  $\beta$ -phase, we calculate the  $(\Delta e)^2$  values between such spin monomers, where  $\Delta e$  is the energy split that results when the SOMO's of the two  $(ET)_2^-$  monomers interact. The anti-ferromagnetic spin exchange interaction  $J_{AF}$  between two spin monomers is related to the associated  $(\Delta e)^2$  value as<sup>21,22</sup>

$$J_{AF} = -\frac{(\Delta e)^2}{U^{eff}}$$

Since the effective on-site repulsion  $U^{eff}$  is nearly constant in a given system, the trends in the  $J_{AF}$  values are approximated by those in the corresponding  $(\Delta e)^2$  values. Our calculations of the  $(\Delta e)^2$  values for the various spin exchange paths of the  $\beta$ -phase shown in Figure 5 are summarized in Table 3. The strongest  $(\Delta e)^2$  values form uniform chains along the *b*-direction, and the interactions between these chains are weak. Therefore, the magnetic properties of the  $\beta$ -phase should be described by a Heisenberg uniform 1D anti-ferromagnetic chain.

The  $\beta_y$  values calculated for the  $\beta'$ -phase are presented in Table 2b. In contrast to the case of the  $\beta$ -phase, there is no strong dimerization in the donor layer in the  $\beta'$ -phase. The

**Table 2.** HOMO-HOMO interaction energies  $\beta_{ij}$  (in meV) between the nearest-neighbor ET molecules in the donor molecular layers of  $\beta$ - and  $\beta'$ -phases of  $(BEDT-TTF)_2[(IBr_2)_{0.2}(BrCl)_{0.1}(ICl_2)_{0.7}]$

(a) $\beta$ -phase	
Intrastack	Interstack
<i>b</i> = 501	<i>a</i> = 63
<i>b'</i> = 34	<i>a'</i> = 63
	<i>c</i> = 185
	<i>c'</i> = 87
(b) $\beta'$ -phase	
Intrastack	Interstack
<i>b</i> = 35	<i>a</i> = 270
<i>b'</i> = 62	<i>a'</i> = 270
	<i>c</i> = 115
	<i>c'</i> = 146

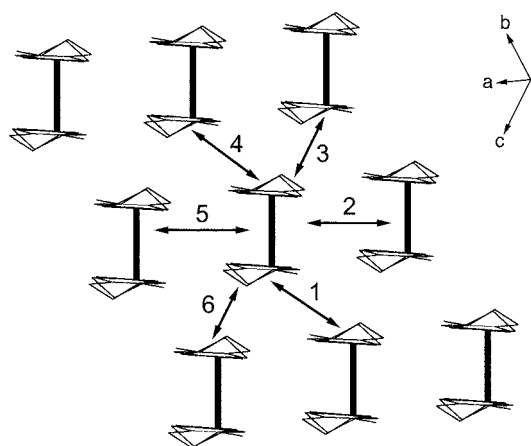


**Figure 5.** Spin exchange paths 1-6 in the donor molecule layer of the  $\beta'$ -phase. The spin monomers are the  $(\text{ET})_2^-$  units linked by thick solid lines.

**Table 3.**  $(\Delta e)^2$  values calculated for various spin exchange paths of the  $\beta'$ -phase<sup>a</sup>

Path	$(\Delta e)^2$	Relative strength
1	39760	1.00
2	605	0.02
3	1267	0.03
4	39760	1.00
5	605	0.02
6	1267	0.03

<sup>a</sup>The  $(\Delta e)^2$  values are in units of  $(\text{meV})^2$ .

intra-stack interactions are much weaker than the inter-stack interactions. The strongest inter-stack HOMO-HOMO interaction takes place along the **a**-direction, which accounts for the strong dispersion of the HOMO bands along the  $\Gamma \rightarrow X$  (Figure 4a). However, the interactions between adjacent donor molecules along the **(a+b)** direction are also substantial, though weaker than those along the **a**-direction. Consequently, the  $\beta'$ -phase has both 1D and 2D Fermi surfaces. It is of interest to speculate on a possible reason for the resistivity upturn in the  $\beta'$ -phase below 10 K. The 1D Fermi surface may give rise to a charge density wave instability,<sup>23,24</sup> which might cause a pairing distortion along the **a**-axis direction and open a band gap. Alternatively, a strong dimerization of ET molecules might take place along the intra- or inter-stack direction thereby localizing electrons in dimerized units. To explain the origin of the resistivity upturn of the  $\beta'$ -phase below 10 K, it would be necessary to determine its crystal structure below 10 K.

### Concluding Remarks

The  $\beta'-(\text{ET})_2[(\text{IBr}_2)_{0.2}(\text{BrICl})_{0.1}(\text{ICl}_2)_{0.7}]$  phase is a semiconductor, and its half-filled band of the  $\beta'$ -phase is narrow. Therefore, the magnetic insulating state should be more stable than the metallic state in the  $\beta'$ -phase. According to the HOMO-HOMO interaction energies, this arises from the presence of strong dimerization of ET molecules in the

donor layer, which localizes an unpaired spin in each dimerized  $(\text{ET})_2^-$  unit. The spin exchange interactions between these dimerized units indicate that the magnetic properties of the  $\beta'$ -phase should be described by a Heisenberg uniform 1D antiferromagnetic chain. In the metallic  $\beta'-(\text{ET})_2-[(\text{IBr}_2)_{0.2}(\text{BrICl})_{0.1}(\text{ICl}_2)_{0.7}]$  phase, its two HOMO bands are partially filled and are more dispersive than those of the  $\beta'$ -phase. The partially filled bands of the  $\beta'$ -phase lead to both 1D and 2D Fermi surfaces. The HOMO-HOMO interaction energies of the  $\beta'$ -phase show that there is no strong dimerization in the donor molecule layer, the intra-stack interactions are much weaker than the inter-stack interactions, and the inter-stack interactions are substantial in two different directions of the donor molecule layer. Consequently, the  $\beta'$ -phase has both 1D and 2D Fermi surfaces.

**Acknowledgments.** This work at KHU was supported by the Korea Research Foundation Grant funded by the Korean Government (MOEHRD) (KRF-2005-003-C00086). M.-H. W. thanks the support by the Office of Basic Energy Sciences, Division of Materials Sciences, U. S. Department of Energy, under Grant DE-FG02-86ER45259.

### References

- Williams, J. M.; Ferraro, J. R.; Thorn, R. J.; Carlson, K. D.; Geiser, U.; Wang, H. H.; Kini, A. M.; Whangbo, M.-H. *Organic Superconductors (including Fullerenes): Synthesis, Structure, Properties and Theory*. Prentice Hall: New Jersey, 1992.
- Williams, J. M.; Wang, H. H.; Beno, M. A.; Emge, T. J.; Sowa, L. M.; Copps, P. T.; Behrooz, F.; Hall, L. N.; Carlson, K. D.; Crabtree, G. W. *Inorg. Chem.* **1984**, *23*, 3839.
- Wang, H. H.; Beno, M. A.; Geiser, U.; Firestone, M. A.; Webb, K. S.; Nuñez, L.; Crabtree, G. W.; Carlson, K. D.; Williams, J. M.; Azevedo, L. J.; Kwak, J. F.; Schirber, J. E. *Inorg. Chem.* **1985**, *24*, 2465.
- Emge, T. J.; Wang, H. H.; Leung, P. C. W.; Rust, P. R.; Cook, J. D.; Jackson, P. L.; Carlson, K. D.; Williams, J. M.; Whangbo, M.-H.; Venturini, E. L.; Schirber, J. E.; Azevedo, L. J.; Ferraro, J. R. *J. Am. Chem. Soc.* **1986**, *108*, 695.
- Emge, T. J.; Wang, H. H.; Bowman, M. K.; Pipan, C. M.; Carlson, K. D.; Beno, M. A.; Hall, L. N.; Anderson, B. A.; Williams, J. M.; Whangbo, M.-H. *J. Am. Chem. Soc.* **1987**, *109*, 2016.
- Yoneyama, N.; Miyazaki, A.; Enoki, T.; Saito, G. *Synth. Met.* **1997**, *86*, 2029.
- Mori, T. *Bull. Chem. Soc. Jpn.* **1998**, *71*, 2509.
- Laukhina, E.; Tkacheva, V.; Chekholov, A.; Yagubskii, E.; Wojciechowski, R.; Ulanski, J.; Vidal-Gancedo, J.; Veciana, J.; Laukhin, V.; Rovira, C. *Chem. Mater.* **2004**, *16*, 2471.
- Buravov, L. I.; Zvarykina, A. V.; Ignat'ev, A. A.; Kotov, A. I.; Laukhin, V. N.; Makova, M. K.; Merzhanov, V. A.; Rozenberg, L. P.; Shibaeva, R. P.; Yagubskii, E. B. *Bull. Acad. Sci. USSR (Engl.)* **1988**, 1825.
- Whangbo, M.-H.; Hoffmann, R. *J. Am. Chem. Soc.* **1978**, *100*, 6093.
- Wang, H. H.; VanZile, M. L.; Schlueter, J. A.; Geiser, U.; Kini, A. M.; Sche, P. P.; Koo, H.-J.; Whangbo, M.-H.; Nixon, P. G.; Winter, R. W.; Gard, G. L. *J. Phys. Chem. B* **1999**, *103*, 5493.
- Koo, H.-J.; Whangbo, M.-H.; Dong, J.; Olejniczak, I.; Musfeldt, J. L.; Schlueter, J. A.; Geiser, U. *Solid State Commun.* **1999**, *112*, 403.
- Ward, B. H.; Schlueter, J. A.; Geiser, U.; Wang, H. H.; Morales, E.; Parakka, J. P.; Thomas, S. Y.; Williams, J. M.; Nixon, P. G.; Winter, R. W.; Gard, G. L.; Koo, H.-J.; Whangbo, M.-H. *Chem.*

- Mater.* **2000**, *12*, 343.
14. Jones, B. R.; Olejniczak, I.; Dong, J.; Pigos, J. M.; Zhu, Z. T.; Garlach, A. D.; Musfeldt, J. L.; Koo, H.-J.; Whangbo, M.-H.; Winter, R. W.; Mohtasham, J.; Gard, G. L. *Chem. Mater.* **2000**, *12*, 2490.
15. Schlueter, J. A.; Ward, B. H.; Geiser, U.; Wang, H. H.; Kini, A. M.; Parakka, J.; Morales, E.; Koo, H.-J.; Whangbo, M.-H.; Winter, R. W.; Mohtasham, J.; Gard, G. L. *J. Mater. Chem.* **2001**, *11*, 2008.
16. Dai, D.; Ren, J.; Liang, W.; Whangbo, M.-H. *Crystal and Electronic Structure Analysis Using CAESAR 2.0*; 2002. (This program can be downloaded free of charge from the website, <http://chvamw.chem.ncsu.edu/>).
17. Whangbo, M.-H.; Williams, J. M.; Leung, P. C. W.; Beno, M. A.; Emge, T. J.; Wang, H. H.; Carlson, K. D.; Crabtree, G. W. *J. Am. Chem. Soc.* **1985**, *107*, 5815.
18. Williams, J. M.; Wang, H. H.; Emge, T. J.; Geiser, U.; Beno, M. A.; Leung, P. C. W.; Carlson, K. D.; Thorn, R. J.; Schultz, A. J.; Whangbo, M.-H. *Prog. Inorg. Chem.* **1987**, *35*, 51.
19. Mott, N. F. *Metal-Insulator Transitions*; 2nd ed.; Taylor & Francis: New York, 1990.
20. Whangbo, M.-H. *J. Chem. Phys.* **1970**, *70*, 4963.
21. Whangbo, M.-H.; Koo, H.-J.; Dai, D. *J. Solid State Chem.* **2003**, *176*, 417.
22. Whangbo, M.-H.; Dai, D.; Koo, H.-J. *Solid State Sci.* **2005**, *7*, 827.
23. Moret, R.; Pouget, J. P. In *Crystal Chemistry and Properties of Materials with Quasi-One-Dimensional Structures*; Rouxel, J., Ed.; Reidel: Dordrecht, The Netherlands, 1986; p 87.
24. Canadell, E.; Whangbo, M.-H. *Chem. Rev.* **1991**, *91*, 965.
-